https://doi.org/10.3311/PPci.39737

Periodica Polytechnica Civil Engineering

Insights into Pipe Jacking-induced Ground Deformation Considering Dynamic Cutter Excavation Effect through Numerical Modelling

Qixiang Yan[1], Minjie Qiao[1], Chuan Zhang[1*], Zhengyu Xiong[1], Yifeng Zhang[2], Jie Huang[3]

[1] State Key Laboratory of Intelligent Geotechnics and Tunnelling, Southwest Jiaotong University, 111 Section 1, North 2nd Ring Road, Jiulidi Street, 610031 Chengdu, China
[2] Zachry Department of Civil & Environmental Engineering, Texas A&M University, 400 Bizzell St., TX 77843 College Station, USA
[3] Guangzhou Metro Construction Management Co., Ltd., 1238 Xingang East Road, 510220 Guangzhou, China
[*] Corresponding author, e-mail: zhangchuan@my.swjtu.edu.cn

Received: 28 December 2024, Accepted: 10 April 2025, Published online: 17 April 2025

Abstract

The pipe jacking method has been increasingly applied to a variety of tunnel projects. Investigating the ground disturbance characteristics during pipe jacking is of great significance to ensure accurate safety assessment and timely ground deformation control. This paper developed a three-dimensional model to simulate the entire pipe jacking process of a shallow-buried cross passage tunnel in soft strata. A key contribution of this research is the development of an element shear failure approach, combining element failure method with shear failure modeling. Meanwhile, the dynamic cutter excavation effect and the soil shear failure were considered in the numerical modeling. Through the comparison with the field monitoring results and traditional numerical simulation approach, the effectiveness, reliability, and superiority of the proposed approach were well demonstrated. Moreover, based on the numerical results, the ground deformation characteristics along with the stress-strain state of the cutter head during the soil excavating process were thoroughly analyzed. The proposed approach and its application in the ground disturbance analysis will offer useful references and guidance for numerical studies in similar pipe jacking projects in near future.

Keywords

pipe jacking, ground displacement, numerical modeling, finite element method, soil dynamic shear failure

1 Introduction

With the continuous development of urbanization and rapid advancement of mechanized construction, the utilization of vast underground space has received increasing attention [1–4]. As a promising trenchless tunneling method that boasts the advantages of high efficiency, safe construction, seepage resistance, and broad applicability to a variety of strata, the pipe jacking method has been widely applied to numerous municipal projects such as drainage pipelines, underground utility corridors, subway entrances, and metro crossing passages [5, 6]. The pipe jacking method can be described as a technique of using hydraulic rams to push precast sections to line a tunnel excavated by a cutting head or shield [7]. During the implementation of the pipe jacking method, the starting and receiving shafts are constructed first at both ends of the designed tunnel. Shortly after the shafts are excavated, a powerful hydraulic jacking rig and a tunneling machine are put into position, the jacking rig then applies a proper thrusting force that pushes the tunneling machine against the supporting wall of the starting shaft and then into the ground. Once the machine reaches a predetermined position in the soil, a pipe segment is lowered into the shaft behind the jacking rig and the tunneling machine. To ensure that the jacking forces are distributed around the circumference of a pipe being jacked, a jacking ring is used to transfer the loads. In the excavation process, the cutter head of the tunneling machine excavates the soil and maintains the stability of the tunnel face simultaneously, and the waste soil is further discharged by the soil conveying system. Each time a pipe segment is fully jacked, the hydraulic jacking system is then retracted and the next segment is lifted into the working shaft to continue the jacking process, with the remaining pipe segments being thrust in sequence until the cutter head reaches the receiving pit. Additionally, it is essential to continuously

Cite this article as: Yan, Q., Qiao, M., Zhang, C., Xiong, Z., Zhang, Y., Huang, J. "Insights into Pipe Jacking-induced Ground Deformation Considering Dynamic Cutter Excavation Effect through Numerical Modelling", Periodica Polytechnica Civil Engineering, 2025. https://doi.org/10.3311/PPci.39737

and synchronously grout pressurized slurry into the annular space between pipe segments and surrounding soils for mitigating the frictional resistance, which is generated by the movement of the pipe segment behind a cutting head that is pushed into ground by hydraulic rams. This is in sharp contrast to the shield tunnel method, in which the shield is thrusted by hydraulic rams instead of the assembled liner. Moreover, compared with the shield tunnel, the pipe jacking tunnel generally has a shallower buried depth, and its entire lining structure has to progress through the surrounding soil, which results in the complicated variation of the ground displacement and great difficulty in controlling the ground surface deformation, consequently causing adverse effects to the jacking efficiency, strata stability, and adjacent infrastructures. Therefore, it is of great significance to study the ground disturbance effect of the pipe jacking tunnel, especially with a shallow buried depth.

So far, numerous researchers have made many encouraging achievements concerning this topic. These achievements are mainly obtained based on theoretical analysis, field monitoring, and numerical modeling. Through theoretical analysis, the ground disturbance characteristics of pipe jacking construction were analyzed, and the division method of ground disturbance zones was further proposed. Particularly, Peck [8] proposed a series of classical theoretical formulas for predicting the ground displacement conforming to a Gaussian distribution by analyzing a large amount of surface settlement field data and this method has laid a solid foundation for numerous later studies. Niu et al. [9] presented a new theoretical method that combined Mindlin's displacement solution with random medium theory and considered the influence of soil loss, additional stress, and friction. Beckmann et al. [10] introduced a theoretical approach named CoJack that employed nonlinear structural equations and considered the load-distribution effects. From above literature it can be seen that those works provide valuable insights based on multiple theories [11, 12]. However, most of them are dependent on necessary assumptions, greatly affecting their predictive capabilities in practical applications with complicated conditions. Meanwhile, the theoretical analysis hardly considers the intricate dynamics of soil-lining interactions inherent in pipe jacking operations. In addition, by means of field monitoring, many researchers also made extensive achievements based on in-situ data of ground deformation [13], lining internal stress, and pipe jacking parameters in practical engineering projects [14–21]. Farrokh [22] analyzed a large number of field data to acquire the abrasion behaviors of cutters of different sizes and proposed a predictive model of cutters' service life. Li et al. [23] explored the correlation between the jacking control and ground displacement during different stages of pipe jacking construction by comprehensively analyzing the field monitoring data. Yu et al. [24] analyzed a great deal of field data from a box pipe jacking project, and found that the on-site geological conditions, lubricated overcut, work stoppages, and deviations in alignment have a great influence on jacking force. Zhang et al. [25] explored the soil deformation mechanism in the construction of curved pipe jacking by considering layered displacement, ground deformation, and transversal deformation of deep soil. It is confirmed that the field monitoring surely offers real-time data but is constrained by the specific spatial and temporal coverage, making it challenging to comprehensively grasp the ground's complex behaviors.

In contrast, numerical modeling empowers researchers with the ability to simulate a wide array of scenarios, incorporating various soil properties, pipe geometries, and operational parameters. Through numerical simulations, intricate phenomena such as soil-lining interaction, ground displacement, and stress redistribution can be meticulously analyzed, providing crucial insights for optimizing jacking operations, mitigating risks, and enhancing the overall efficiency and safety of underground infrastructure projects. Because of the advantages that FEM modeling leverages mesh-based discretization techniques, allowing for efficient representation of soil-pipe interactions while maintaining reasonable computational overhead, many researches primarily adopted the finite element method to simulate the pipe jacking process [26–29]. Gong et al. [30] constructed a sophisticated numerical model of parallel rectangular pipe jacking and analyzed the ground displacement pattern. Batsaikhan et al. [31] conducted a novel numerical analysis to investigate the applicability of the pipe jacking technique considering different inclination angles and high wall slopes. Ma et al. [32] established an elaborate numerical model verified with field monitoring to interpret the soil disturbance areas in pipe jacking construction. Zhang et al. [33] also established a sophisticated pipe jacking model to analyze the mechanical behaviors of supporting structures at different distances. Liu et al. [34] combined numerical simulations and full-scale tests to analyze the influence of joint deflection on the axial stress distribution and jacking load transfer of pipe jacking. Zhang et al. [35] combined conditional random field (CRF) and Co-Kriging theory to establish a numerical model and then used unconditional random field (URF) method to verify the reliability and applicability of the proposed model. Li et al. [36] further constructed a soil-structure elastic-plastic model to analyze the spatio-temporal evolution of ground displacements. Pan et al. [37] constructed a sophisticated Plaxis two-dimensional finite element model to analyze the influence of pipe jacking construction on deformation of ambient structures. The above researches well contribute to a deep understanding of mechanical characteristics, controlling factors, and ground deformation of pipe jacking, and provide a solid foundation for numerical modeling of the pipe jacking process. However, there are still several limitations of current numerical studies on the pipe jacking-induced ground disturbance:

1. Most of these models failed to consider the dynamic interaction between pipe jacking cutter and soil. Instead, they directly adopted the soil killing element approach and activating the pipe lining elements, which cannot reflect the cutter excavation effect and the positional change of pipe jacking structure in reality.
2. Moreover, in most of the studies, the pipe-soil friction has been directly ignored or simplified by artificially assuming the friction load.
3. Meanwhile, some of those related studies rely on two-dimensional models [38], hardly reflecting the three-dimensional structural stress and strain states in the jacking process.

Aimed at the aforementioned limitations, this paper set out to study the ground disturbance during pipe jacking construction through numerical modeling that fully considers the dynamic interaction between pipe jacking machine and soil. Based on an actual shallow-buried circular pipe jacking project, a sophisticated model was established, which considered the rotation of cutter head, the excavation of soil body, and the progression of pipe-lining. Especially, the element shear failure approach was introduced to better simulate the dynamic soil excavation process by single cutter head, and the numerical results were then compared with the traditional killing element approach. In addition, the horizontal, vertical, and longitudinal ground disturbances of the pipe jacking process were thoroughly analyzed. Finally, the deformation of tunnel face, the dynamic displacement of excavated soil, and the cutter-head stress state were also investigated.

2 Theoretical basis

The ground disturbance during pipe jacking construction arises from the interaction between the pipe jacking and surrounding soil. To facilitate a deeper comprehension of the ground disturbance characteristics induced by pipe jacking, and lay a solid foundation for the subsequent numerical modeling of the ground deformation, Section 2 provided an overview of existing theoretical basis concerning this topic. The soil is mainly influenced by the initial formation stress before the start of pipe jacking. With advancement of the pipe jacking machine, the soil is subjected to both the jack propulsion and excavating forces, causing dynamic stress states due to compression, extrusion, and shear deformation [32]. Throughout the pipe jacking process, disturbance zones are primarily categorized into seven regions based on their relative position to the tunnel face and the disturbance factors, as illustrated in Fig. 1.

After analyzing a large amount of field data, Peck [8] proposed a series of formulas for ground displacement which influenced subsequent generations and became known as Peck formulas. For the first time, Peck comprehensively revealed the definition of ground loss and proposed a calculation approach for predicting the ground surface settlement of tunnels due to excavation. Peck proposed that ground deformation was caused by strata loss, and the theory of an approximate normal distribution of

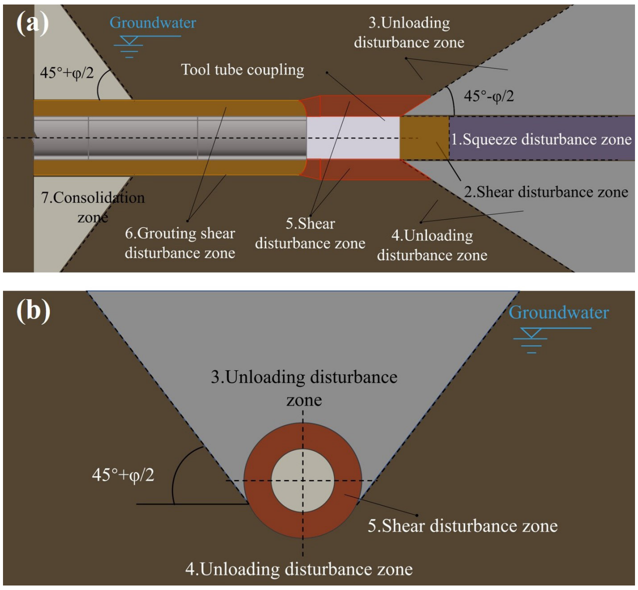

Fig. 1 Disturbance zones of circular jacking pipe construction: (a) longitudinal section; (b) cross section

settlement troughs along the horizontal direction was also illustrated. The classical theoretical formulas have laid a solid foundation for a great deal of later researches. Equations (1) to (3) are specified as follows:

$$S_{\max} = \frac{V_{loss}}{i\sqrt{2\pi}}, \tag{1}$$

$$S(x) = S_{\max} e^{-\frac{x^2}{2i^2}}, \tag{2}$$

$$S(x) = S_0 + S_{\max} e^{-\frac{x^2}{2i^2}}, \tag{3}$$

where $S(x)$ means the amount of ground displacement, V_{loss} stands for the amount of body loss per unit length of the tunnel as a coefficient of the width of the ground displacement channel, x represents the horizontal distance from the centerline of the pipe, i is the width coefficient, S_{max} means the maximum displacement above the tunnel axis, S_0 is the consolidated displacement of ground settlement trough.

3 Numerical modeling

3.1 Engineering background

Section 3.1 took a shallow-buried pipe jacking project for constructing a station entrance passage in Guangzhou Metro as an engineering background. The entire project is exhibited in Fig. 2. Fig. 2 (a) illustrates pipe jacking construction method while Fig. 2 (b) is an enlarged view of the pipe jacking machine. Meanwhile, the top view and the longitudinal view are depicted in Fig. 2 (c) and (d) separately. The physical and mechanical properties of the ground soil are shown in Table 1. According to the geological data, the tunnel excavation mainly passes through the silty fine sand layer. The pipe-jack tunnel has a buried depth of 4.00 m, an outer diameter of 3.00 m, and a wall thickness of 0.15 m. The pipe jacking machine has a total length of 7.50 m.

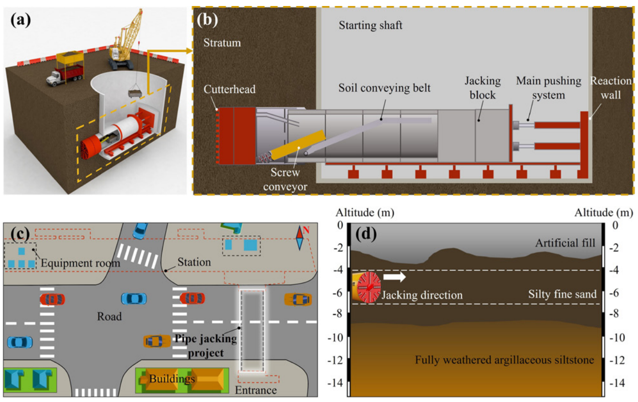

Fig. 2 Overall situation: (a) pipe jacking method; (b) pipe jacking machine; (c) top view; (d) longitudinal view

3.2 Model establishment

Considering the disturbance range and calculation cost of pipe jacking construction, the model, which is shown in Fig. 3, was designed as 16.00 m long, 10.00 m wide, and 16.00 m high. The geometric parameters of the pipe jacking were exactly determined according to the project prototype in the Guangzhou Metro. The ground and pipe jacking models were assigned by the three-dimensional hexahedron elements (C3D8R). The entire finite element model consisted of 2.35×10^5 elements. Because the lining material adopted C50 precast reinforced concrete, with a stiffness much greater than that of the surrounding soil. Hence, it was assumed that no plastic deformation occurs during the construction process, thus the linear elastic constitutive model was employed. In addition, the shear failure model was employed to simulate the soil's nonlinear mechanical behaviors. Roller fixities were used for the lateral and bottom boundary conditions to provide stability for the soil mass. For the pipe jacking section exposed outside the soil, the bottom nodes were fixed using roller fixities. The steel shell of pipe jacking machine was not considered alone. The pipe section adopted isotropic homogeneous elastic material, and the joint effect of the pipe section was ignored. Fig. 3 (c) shows the model of the cutter head. The cutter head was pane-type with an opening ratio of 67.00%, considering only the center cutter and cutters. The stiffness of the cutter head was generally much greater than that of the soil and pipe section. Thus, its deformation was ignored and the model of the cutter head was set as a rigid body. In addition, the pointing of the directions that were mentioned in the article is also shown in Fig. 3.

The operational parameters of cutter head in numerical modeling were determined according to the field data.

Table 1 Physical and mechanical parameters of different ground layers

Ground layer	Natural gravity (kN/m^3)	Young modulus (MPa)	Internal friction angle (°)	Cohesive force (kPa)	Thickness (m)	Poisson ratio
Artificial fill	17.50	4.50	12.00	10.00	3.00	0.30
Silty fine sand	19.00	6.00	25.00	6.00	6.00	0.29
Fully weathered argillaceous siltstone	21.50	36.00	22.00	34.00	12.00	0.25

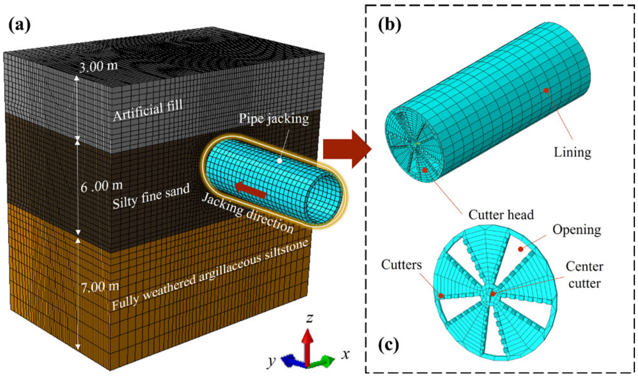

Fig. 3 Finite element model: (a) holistic model; (b) pipe jacking model; (c) cutter head model

Specifically, the rotation angular velocity and the longitudinal jacking speed were applied at the central reference point of the cutter head, meanwhile, the longitudinal jacking speed was applied at the end of the pipe section. The reference penetration was set to 30.00 mm/r. In order to improve computational efficiency, cutter head speed and tunneling speed were amplified appropriately. The final cutter head speed was 0.63 rad/s (6.00 r/min) while the jacking speed was 0.003 m/s (18.00 cm/min). A uniformly distributed radial grouting pressure was applied on the excavation surface, and the grouting pressure was set to 0.08 MPa. The surface-to-surface contact was set both at the interface between cutter head and soil units and that between pipe section and soil units. The friction coefficient was also set in the tangent direction based on the penalty function method. The friction coefficient between the cutter head surface and soil was 0.10, and that between the pipe section surface and soil was 0.25.

3.3 Element shear failure approach

Traditionally, the killing element approach is adopted to simulate the tunnel excavation effect. However, this approach neglects the element state and involves multiplying the stiffness of the specific area element by a minimal reduction coefficient. Then, the killed element stress and strain are reset to 0, while the stiffness matrix size remains constant. The killing element approach is simple to operate. Although this approach is widely used, it significantly diverges from the actual situation, resulting in inadequacy for simulating the continuous rotation of the cutter head and the excavated soil at the tunnel face. This is because, during the actual pipe jacking construction process, the soil at the tunnel face is continuously and dynamically removed under high shear stresses. In order to realistically simulate this scenario, the element shear failure approach is introduced. The element shear failure approach is essentially a combination of the element failure method and the failure model (the shear failure model is adopted in this study). On one hand, for the purpose of simulating the disappearance or completely failed elements of the material in real situations, the element failure method is proposed based on the FEM. On the other hand, the failure model is commonly employed to characterize the destructive behavior of materials. For example, the shear failure model is applied to evaluate the performance of elements experiencing shear stresses. Particularly, the shear failure model is useful for simulating materials prone to failure under high shear conditions. ABAQUS offers material-based shear failure models that define damage evolution rules based on stress or strain. Indeed, the combined approach incorporating both element failure method and failure modeling has been extensively implemented in various engineering applications. Padilla-Llano et al. [39] combined the element failure method with plastic strain model to simulate the cyclic fracture characteristics of structural steel. So as to research the property of laminated glass, Wang and Zhupanska [40] proposed a novel element failure approach and integrate it into finite element analysis (FEA) to study the lightning heat transfer in situation of the moving boundary. Zhang et al. [41] conducted a damage analysis to simulate crack propagation in UHPC under shear tension, combining the concrete damage plasticity model with the element failure method. Furthermore, the similar approach is also gradually being adopted in tunnel excavation studies. Han et al. [42] investigated the dynamic construction process of tunnel boring machine (TBM) by employing the element plastic failure approach to model the formation of rock fragments.

During pipe jacking construction, the cutter head rotates at high speed, generating significant shear stresses on the soil at the tunnel face while gradually excavating the soil. This process closely aligns with the application scenario of the previously mentioned element failure method and shear failure model. Therefore, this study combines the element failure method and the shear failure model, calling it the element shear failure approach to simulate the pipe jacking construction process. A shear damage model driven by plasticity is adopted. This model is based on the equivalent plastic strain values at the integration points of the elements. The proposed element shear failure approach adopts damage parameter ω to judge whether an element is damaged and uses "status" variable to control the deletion of elements. When the "status" value is 0, the element is deleted from the model. Damage is assumed to occur when the damage parameter ω exceeds 1, and then the "status" would be set to 0. The damage parameter ω is defined as follows:

$$\omega = \frac{\bar{\varepsilon}_0^{pl} + \sum \Delta \bar{\varepsilon}^{pl}}{\bar{\varepsilon}_f^{pl}}, \tag{4}$$

where $\bar{\varepsilon}_0^{pl}$ is any initial value of the equivalent plastic strain. where $\Delta\bar{\varepsilon}^{pl}$ is the increment of the equivalent plastic strain. where $\bar{\varepsilon}_f^{pl}$ is strain at destruction. The damage parameter ω is calculated based on the equivalent plastic strain values at the element integration points. For the stress-strain relationship and ω, they are mutually influencing. Essentially, the main purpose of introducing the damage parameter ω is to determine whether the element has failed completely or not.

The main steps of the element shear failure approach are as follows. Firstly, the shear failure criterion and damage parameter ω are defined for the soil element material. Then the damage variable is acquired and assigned to the element state parameter "status" (Boolean type) to determine whether the element has completely failed. If the failure criterion is reached, the element is then deleted from the model and no longer participates in the subsequent computation. Through this approach, the entire dynamic process of tunnel face soil was modeled, including, excavating, evolving damage, and ultimate failure. The complete procedures are exhibited in Fig. 4.

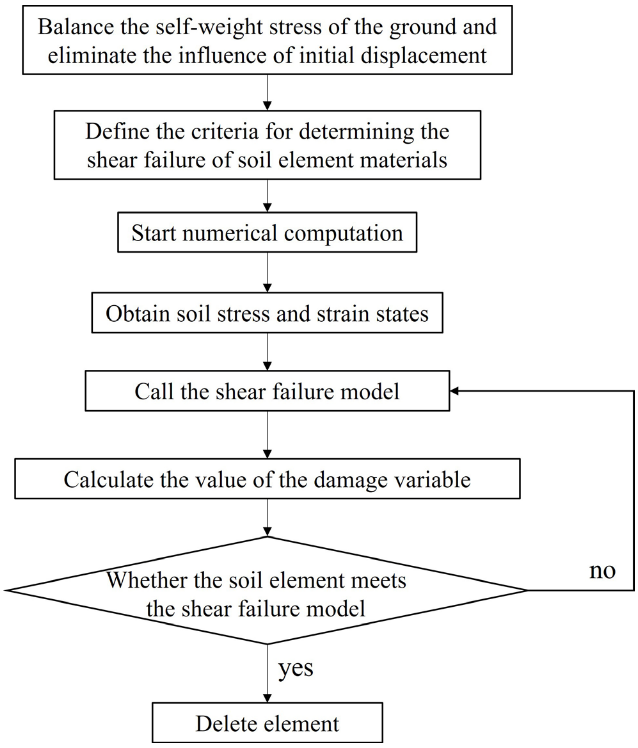

Fig. 4 Process of the element shear failure approach

4 Results and analysis

4.1 Comparative analysis and model verification

To verify the effectiveness and reliability of the proposed model, the numerical results of ground surface deformation were compared to the field monitoring data. In this project, the ground surface displacements along the tunneling central axis and its normal line were continuously monitored. Moreover, the comparative analysis of results from the direct killing element approach and the dynamic element shear failure approach was also performed. Particularly, in order to verify the applicability, the result from the proposed approach was fitted with the Peck formulas. Fig. 5 depicts the curves of ground surface horizontal and vertical displacements in the cross section 0.3 m ahead of the tunnel face based on the two numerical simulation approaches. Fig. 5 (a) and (b) depict the horizontal displacement curves, while Fig. 5 (c) and (d) present the vertical displacement curves. The bar indicates the error between the numerical and field monitoring data. As observed, both the numerical

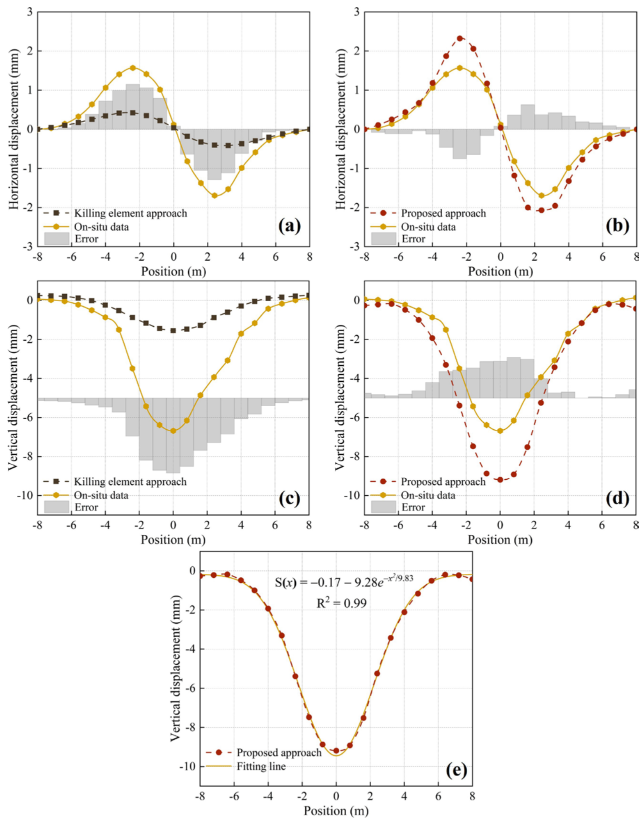

Fig. 5 Comparison of displacement results from the two different approaches with field data

approaches yielded similar results whether in the horizontal or vertical displacement. However, the proposed approach aligned more closely with field data. By observing the error, it's apparent that the field data curve exhibited less deviation with the proposed approach compared to the killing element approach, for both horizontal and vertical displacements. This difference was most evident in the horizontal displacement. By comparison, the killing element approach showed a maximum error of over 1 mm, and most of bars exceeded 0.5 mm. This was in a sharp contrast to the distributed error bars from the proposed approach, with 75% of them lower than 0.45 mm. Similar phenomenon could also be observed from the vertical displacement. The killing element approach showed errors reaching up to 4.2 mm, with the majority of errors exceeding 2.0 mm, which was much higher than that from the element shear approach. It is worth pointing out that although the element shear approach is closer to the field data, there is still some error between them. The error originates from boundary effect, as well as model simplification and the idealization of construction parameters. However, despite the error between the numerical simulation results and the field-measured values, the proposed approach clearly provides a reasonable prediction and trend analysis of ground settlement in pipe jacking construction. Fig. 5 (e) demonstrates the fitting result of the proposed approach with the Peck formulas. The two curves overlapped with an R^2 value of 0.99. This phenomenon indicated that the proposed approach fitted the Peck formulas exceptionally well, which demonstrated the effectiveness and reliability of both the proposed approach and the numerical model. Hence, based on the comparative analysis, it could be concluded that the modeling was reliable. Meanwhile, the proposed approach better agreed with the actual situation and displayed evident superiority over the killing element approach.

Subsequently, a comparative analysis was also conducted for the displacements along the longitudinal axis (pipe jacking direction). Due to a lack of relevant measured data, only numerical results were compared. Fig. 6 shows the ground longitudinal displacement distributions from both the killing element approach and the proposed approach. Overall, the distribution characteristics of the longitudinal displacement acquired from both approaches had a good consistency. Both approaches observed a symmetric displacement distribution along the tunneling center axis. In addition, the maximum displacements approximately appeared at the center point of the tunnel face. Nevertheless, the longitudinal displacement from the killing element approach was excessively small, with its value even lower than 1.15×10^{-3}. In contrast, the numerical results

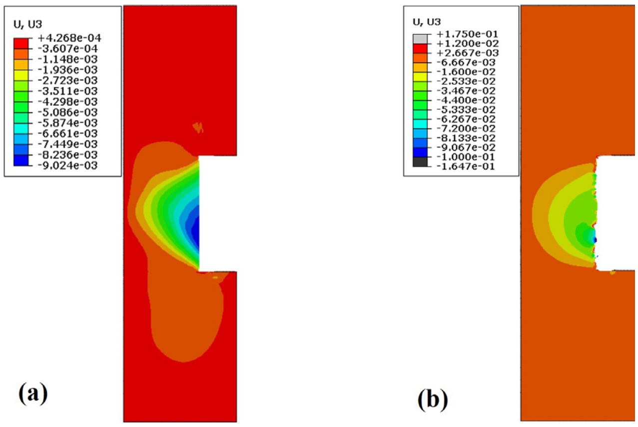

Fig. 6 Longitudinal displacement: (a) killing element approach; (b) proposed approach

from the proposed approach were in a much more reasonable range. Additionally, it was visualized from Fig. 6 (b) that some inconsistent displacements were scattered at the tunnel face. This phenomenon could be attributed to the dynamic soil excavation effect. Therefore, the reasonability of the proposed approach was well reflected.

To better compare the numerical results of the two different modeling approaches, the underground displacements in the disturbed regions around the tunnel face were extracted and analyzed. Specifically, four different regions were concentrated, regions a and b refer to the transverse sections 2.0 m above and below the tunnel horizontal centerline, respectively, while regions c and d represent the cross sections at distances of 3.0 m and 6.0 m to the right of the tunnel vertical centerline, respectively. The regions a and b were primarily selected to study the differences in the results of both approaches around the tunnel face, while regions c and d were extracted to analyze ground disturbance at different depths. The results are exhibited in Figs. 7 and 8. Fig. 7 displays the distributed vertical displacements in regions a and b based on the killing element approach and the element shear failure approach. Meanwhile, Fig. 8 compares the curves of longitudinal displacements in regions c and d. As observed from Fig. 7, both the displacement curves from the two approaches were symmetrically distributed about the tunnel centerline. However, the vertical displacement resulting from the element shear failure approach varied much more significantly than that from the killing element approach. The maximum settlement in region a for the former approach reached up to 8.8 mm, which was in sharp contrast to a value of 1.2 mm at the same position for the latter approach. Similarly, the proposed approach also yielded a larger uplift at the bottom of the tunnel face.

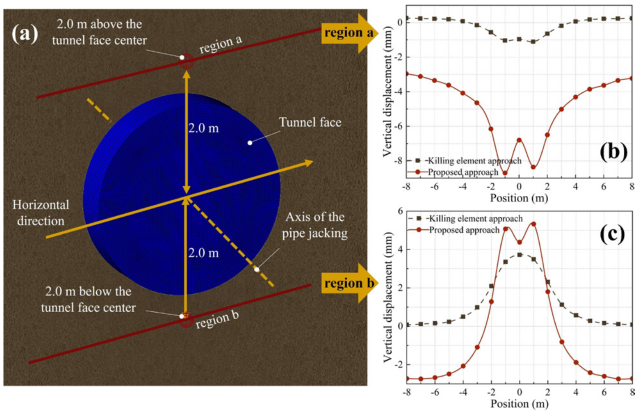

Fig. 7 Vertical displacement: (a) disturbed regions around the tunnel face; (b) 2 m above; (c) 2 m below

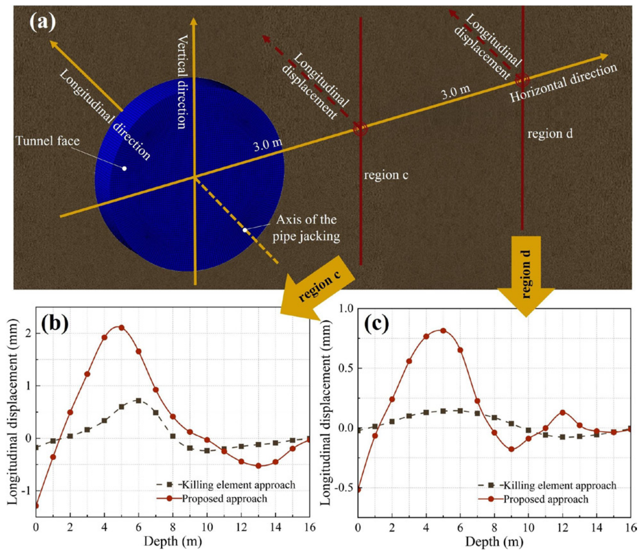

Fig. 8 Longitudinal displacement: (a) disturbed regions around the tunnel face; (b) 3 m to the right; (c) 6 m to the right

The maximum displacement reached 5.4 mm, as compared to 3.7 mm by the counterpart approach. Notably, based on the results of the proposed approach, the curves of vertical displacement presented a W-shaped distribution around the top and bottom regions of the tunnel face. The area with the largest displacement appeared on both sides of the vertical centerline. This phenomenon could be attributed to the arch effect induced by the soil extrusion and excavation during pipe jacking. The arch effect is a structural phenomenon where soil forms an arch-like structure, redistributing overlying loads to the sides. This redistribution reduces settlement at the center while increasing it at the edges, resulting in a W-shaped ground settlement curve [43–45]. The above analysis demonstrated that the killing element approach was relatively unfavorable, as it greatly underestimated the ground deformation throughout the pipe jacking tunneling process, adversely affecting the safety assessment and deformation control. This conclusion could also be supported by Fig. 8, which shows the longitudinal displacement primarily occurred within the depth range of 0.0–16.0 m below the ground surface. Moreover, it was also evident that the proposed approach yielded greater displacement than that of the killing element approach. Therefore, the proposed approach could better reflect the ground deformation characteristics.

4.2 Ground disturbance analysis

Aiming to better understand the disturbed regions in the dynamic excavation process, the ground displacements were extracted and analyzed by adopting the element shear failure approach. Fig. 9 shows the ground surface displacements caused by the pipe jacking construction.

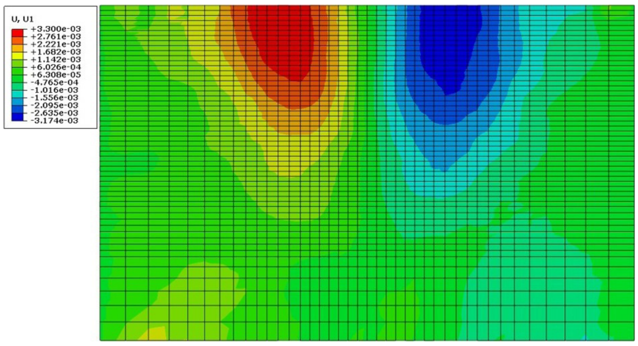

(a)

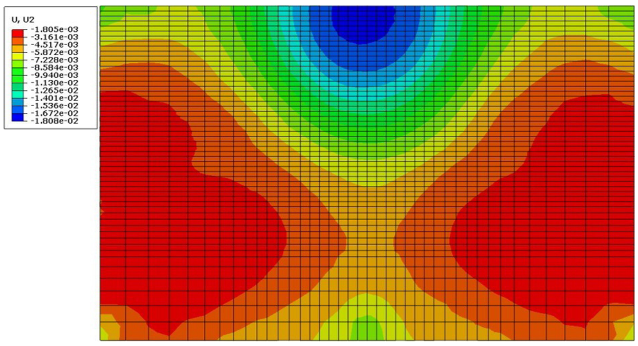

(b)

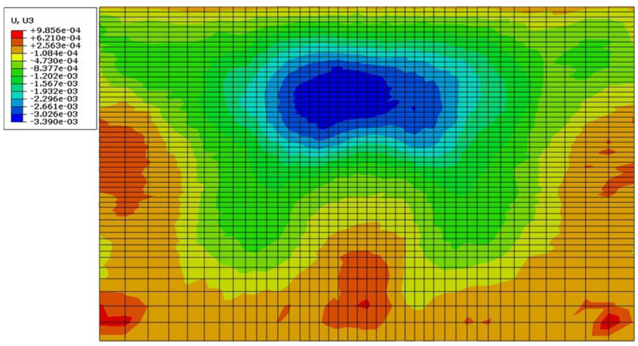

(c)

Fig. 9 Ground surface displacements: (a) horizontal displacement; (b) vertical displacement; (c) longitudinal displacement

As observed, there was a degree of similarity in the spatial distribution of displacements in all directions. Specifically, it showed a symmetric distribution along the tunneling center axis, whether in the horizontal, vertical, or longitudinal directions. However, due to the rotation of the cutter head, the longitudinal displacement distribution on both sides of the axis had a certain difference. Meanwhile, it was notable that there was a trend of moving back in the longitudinal direction around the tunnel face. And the maximum of the longitudinal displacement reached up to 3.39 mm. This phenomenon was due to the clockwise rotation of the cutter head during pipe jacking, which drove the soil downward on the right side, making it easier for the soil in front of the tunnel face to surge into the hole. Thus, the soil above the tunnel face was driven to move back. In addition, the maximum displacement, which reached up to 18.1 mm, occurred in the vertical direction.

The displacements in Z = 1.2 m cross-section disturbed regions were extracted and analyzed in Fig. 10. −0.9 m – 1.2 m means the distance between the tunnel face and Z = 1.2 m cross-section. The negative distance means that the tunnel face has not yet reached the Z = 1.2 m cross-section. As observed, both displacements yield similar results, showing a symmetric distribution along the center axis, whether in the vertical or longitudinal displacements. Almost all the displacements were settlements. In addition, from Fig. 10 (a), it was evident that the maximum of the vertical displacements occurred in the center axis. The maximum displacement was gradually increasing in the excavation process and eventually reached up to approximately 16.8 mm. This was in a sharp contrast to the longitudinal displacement, with a maximum of merely 2.4 mm. Moreover, the peak line in Fig. 10 (b) existed fluctuations. Although there were fluctuations in the peak line, the ground surface displacements were essentially stable after the tunnel face passed through the Z = 1.2 m region.

Fig. 11 shows the variation of ground surface displacement distribution during the jacking process. The target

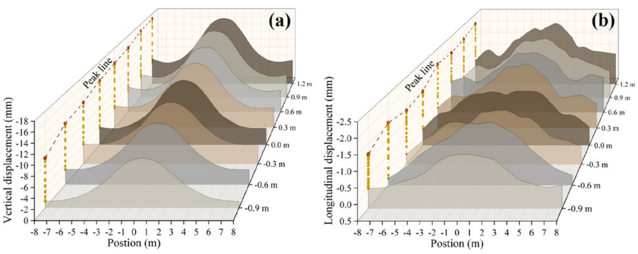

Fig. 10 Distribution of ground surface displacement: (a) vertical displacement; (b) longitudinal displacement

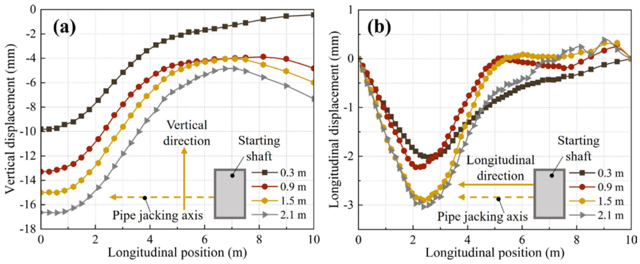

Fig. 11 Variation of ground surface displacement distribution: (a) vertical displacement; (b) longitudinal displacement

tunnel face was chosen at a location 10.0 m from the beginning of the start. Different excavation distances, such as 0.3 m, 0.9 m, 1.5 m, and 2.1 m, were extracted for analysis. It was evident that the curves yielded similar tendencies whether in the vertical or longitudinal displacements. Specifically, in Fig. 11 (a), the ground surface displacements above the axis generally increased as the jacking distance increased. However, there was a notable variation in the vertical ground surface displacement as distance from the model boundary increased. The factors included the movement of deep soil ahead of the tunnel face into the tunnel and the longitudinal displacement constraints at the boundaries. This was in a sharp contrast to the longitudinal displacements, with a more manifest V-shaped distribution region. In fact, in Fig. 11 (b), although the ground surface longitudinal displacement values increased gradually during the pipe jacking process, there was a V-shaped region which meant there were some ground surface displacements decreased. The reason was that when the cutter head rotated, the soil at the tunnel face was in contact with the panel. Meanwhile, the soil was subjected to continuous changes in the supporting section, causing irregular changes in the longitudinal direction of the soil at the surface.

By means of selecting five specific points along the Z = 8.0 m cross-section, the aim was to better investigate deep soil disturbance during dynamic pipe jacking construction. The locations of the position points are shown in Fig. 12. The distance between point 2 and the other points is 2.0 m.

The displacements of the five points at different jacking stages were extracted and analyzed. Fig. 13 shows the displacement of deep soil in different jacking stages. The displacements of the position points were recorded and projected onto the vertical plane. The longitudinal distance between the tunnel face and the Z = 8.0 m cross-section was recorded during the pipe jacking process. The negative distance indicated that the tunnel face had not yet reached the Z = 8.0 m cross-section. It was evident that both points

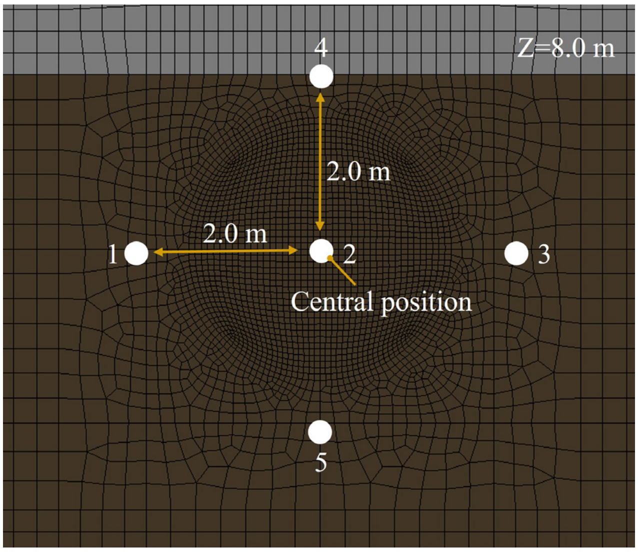

Fig. 12 Location of position point

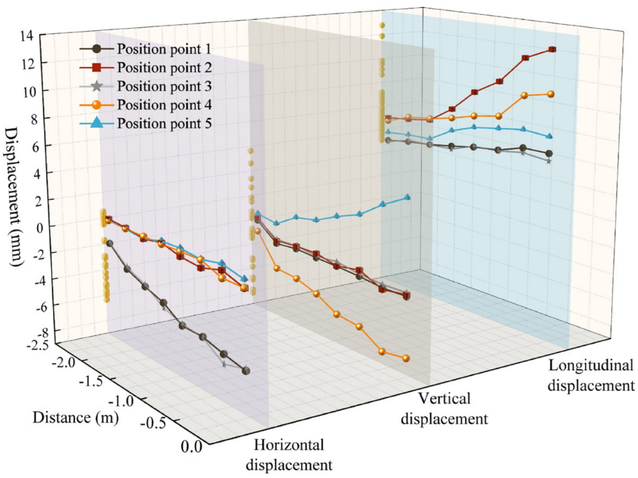

Fig. 13 Displacement of the position points

1 and 3 yielded similar results, whether in the horizontal, vertical, or longitudinal displacements, which indicated that the displacements at these two points were essentially identical. The horizontal displacements at points 1 and 3 were notably larger than other points, reaching up to approximately 6.5 mm, while the longitudinal displacements were considerably small. The displacement direction was also different from the other points. Differently, there were opposite trends at points 4 and 5, especially in the vertical direction. The negative maximum vertical displacement occurred at position point 5, reaching up to nearly 8.1 mm, while the positive maximum vertical displacement occurred at position point 4, reaching up to nearly 3.9 mm. Position point 2 had the largest longitudinal displacement which reached up to approximately 13.0 mm.

Aiming to further understand the relationship between ground disturbance and pipe jacking machine during the jacking process, soil data from $Z = 0.6$ m and $Z = 1.5$ m (tunnel face) cross-sections were extracted and analyzed. In particular, soil displacements within 6 m from the jacking axis were extracted. The results are illustrated in Fig. 14. The positions of $Z = 0.6$ m and $Z = 1.5$ m cross-sections were depicted in Fig. 14 (a) while the directions were shown in Fig. 14 (b). As observed, both the cross-sections yielded similar results that longitudinal displacements of the deep soil at symmetrical positions on both sides of the axis were essentially the same. Meanwhile, the direction of soil displacements at the pipe jacking position was the same as the jacking direction. And the displacements were bigger than the others. Particularly, soil displacements matched the pipe jacking profile very well. This was consistent with the actual situation. In fact, during the pipe jacking process, soil displacements along the surface of the pipe jacking machine certainly were along the surface of the contour. Moreover, with the increase of the horizontal distance from the jacking pipe's axis, the longitudinal displacement of soil gradually decreased. From Fig. 14 (a), in the $Z = 0.6$ m cross-section, which was at a distance of 0.9 m behind the tunnel face, the maximum longitudinal displacement of the soil was approximately 12.0 mm in the center of the arch. From Fig. 14 (b), in the $Z = 1.5$ m cross-section, which was the tunnel face, the longitudinal displacements of the soil in the center of the vault and the inverted arch on the tunnel face were very close, 25.0 mm and 24.0 mm, respectively. Comparing the longitudinal displacement results of the two cross-sections, it was evident that the longitudinal displacement of the deep soil at the center of the tunnel face was approximately twice that of the soil at the same position on the $Z = 0.6$ m cross-section. This indicated that the cutter head had a significant supporting effect on the soil, which was in front of the tunnel face, during excavation. This effect could result in a more prominent impact on the longitudinal displacement of the deep soil. Additionally, the longitudinal displacement of the soil in the central area of the tunnel face was smaller compared to the soil at the edge of

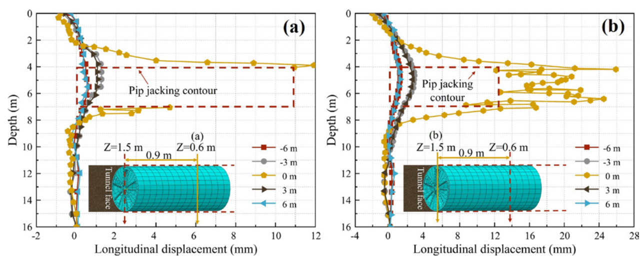

Fig. 14 Longitudinal displacement of the soil along the depth: (a) $Z = 0.6$ m; (b) $Z = 1.5$ m

the cutter head. This phenomenon indicated that there was a tendency of the soil in the central area of the tunnel face to flow into the deeper region.

4.3 Analysis on dynamic excavating process

Studying the dynamic process of pipe jacking construction helps understand the impact on deep soil stability during the excavation, enhances construction safety, and provides valuable experience and guidance for designing similar projects in the future. Thus, in order to better study the dynamic excavating process, the deformation of the tunnel face, the dynamic displacement of excavated soil, and the cutter-head stress state were concentrated and analyzed.

Fig. 15 illustrates the evolution of the tunnel face shape in the first rotation cycle of the cutter head. The calculation of the jacking distance was based on the initial distance between the cutter head and the soil, as well as the jacking speed of the cutter head at the corresponding time. It was evident that the center cutter had penetrated the soil 0.001 m at 1.0 s. At this time, the soil of the vault had a very small displacement along the jacking direction, only reaching 0.7 mm. This was in a sharp contrast to displacement direction of the soil below the tunnel face, with an opposite direction. But the displacements of both regions were close. At 8.0 s, the center cutter penetrated the soil 0.015 m, and the whole cutter head was about to touch the soil of the tunnel surface. The central area of the tunnel face had a significant longitudinal displacement which was caused by the center cutter and reached up to approximately 14.8 mm. At 10.0 s, the center cutter penetrated 0.019 m into the soil, and the whole cutter head penetrated 0.004 m and rotated 72.0° in the soil. At this time, a distinct contour of the cutter head appeared in the tunnel face, which was caused by the rotation of the cutter head. At 11.0 s, the cutter head had rotated 108.0° since the cutter first touched the soil. Meanwhile, the contour of the cutter head continued to develop further. At 18.0 s, the cutter had already rotated one cycle, and the excavation path of the cutter entirely covered the soil on the tunnel face. The positive maximum displacement had reached up to nearly 202.2 mm while the negative maximum displacement had reached up to about 96.0 mm. The complete cycle from the beginning to the 18.0 s was dynamically simulated. The dynamic process of soil changes on the tunnel face was clearly reflected.

Subsequently, the dynamic variation of the cutter head was also concentrated and analyzed in Fig. 16. A specific period was selected to study which was 30.0 s long, from 47.0 s to 77.0 s. At 47.0 s, a small part of the soil body had been removed in the lower half of the cutter head, creating a cavity area. The longitudinal displacement of the soil decreased from inside to outside. When advancing 57.0 s,

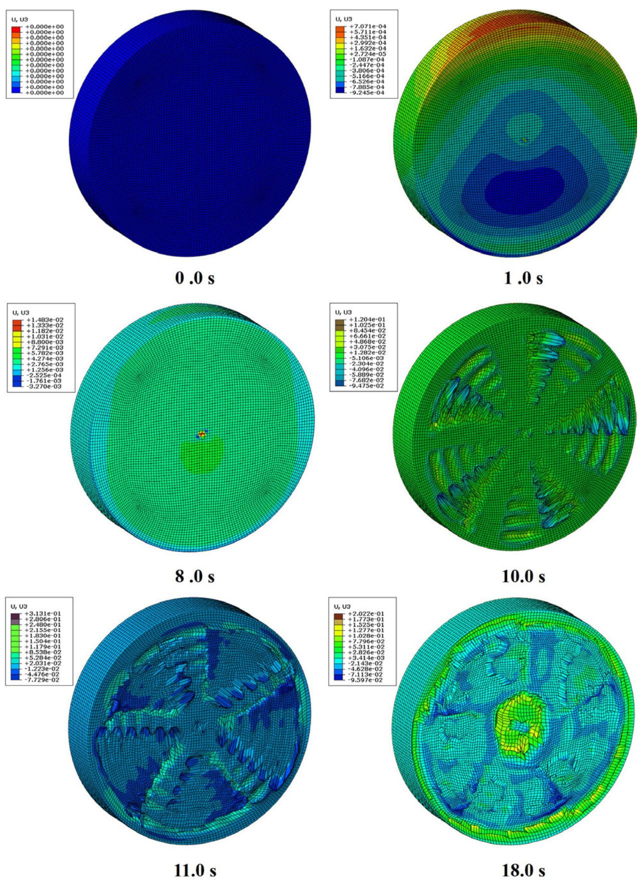

Fig. 15 Dynamic deformation of the tunnel face during a rotation cycle

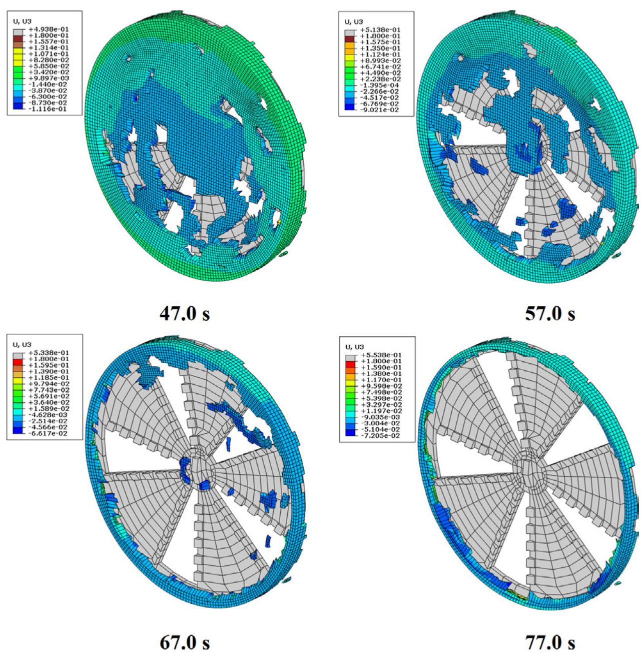

Fig. 16 Dynamic excavation process

the soil in the lower half of the cutter head was removed, only part of the residual soil in the center cutter and the edge area. The cavity area in the upper half of the soil also began to develop. At 57.0 s, the soil in the lower half of the cutter head was removed, leaving only residual soil in the central cutter and the edge area. The cavity area in the upper half of the soil also began to develop. At 67.0 s, the soil in front of the cutter head had been excavated, leaving only a small amount of soil adhering to it. After advancing for 77.0 s, the cutter head had removed all the soil in front of it that was in contact with its surface. Only a small amount of soil remained unexcavated at the edge. Obviously, in this dynamic excavation process, the soil in the lower part of the cutter head will be removed more quickly. Actually, this phenomenon is due to the effect of soil pressure balance. On one hand, the soil pressure increases with depth, creating a gradient that imposes higher pressures on the lower soils. During jacking, these soils with higher pressures are more susceptible to destabilization and damage. On the other hand, the soil in the lower part of the tunnel face is subjected to greater forces and therefore has a greater displacement. It will contact the cutter head earlier in the excavation process and therefore be cut earlier. Thus, as the cutter head advances and continues to cut the soil, the soil in the lower portion of the cutter head is gradually removed, creating a void.

Fig. 17 illustrates the distribution of surface normal contact stress during the excavation process. It was apparent that large normal contact stress was generated near the cutter and at the edge of the panel. This was due to soil penetration and stress concentration caused by geometric mutation. The contact stress between the cutter head surface and the soil was minimal, particularly in the central area of the panel around the center cutter and the other cutters. This was consistent with the reality of the stripped soil pouring into the soil screw conveyor.

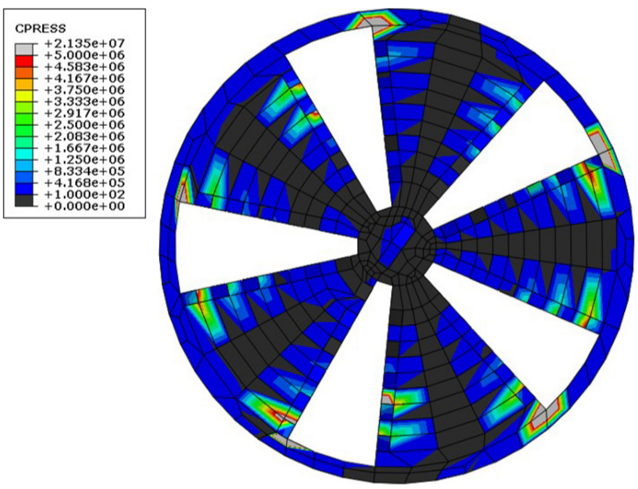

Fig. 17 Normal contact stress of the cutter head

5 Conclusions

The objective of this paper is to investigate the ground disturbance during the dynamic pipe jacking construction. This research introduced an element shear failure approach combining the element failure method and the shear failure model. And a sophisticated numerical model was conducted to simulate the comprehensive pipe jacking process. Especially, ground disturbance during the dynamic excavation process was concentrated. Surface settlement and ground displacement were extracted and analyzed. The dynamic process of soil excavation was simulated and revealed. Major conclusions can be drawn as follows:

1. The numerical results matched well with the classical Peck formulas, which confirmed that the established numerical model could well simulate the pipe jacking construction. The displacement curves from the numerical and theoretical Peck method were highly correlated, with an R^2 value of 0.99. In addition, compared to the traditional approach, the proposed method effectively reflected the dynamic soil excavation process, facilitating a better understanding of ground disturbance characteristics induced by pipe jacking. Specifically, by comparing the numerical results with the field monitoring data, the error of the proposed approach was evidently smaller than that of the killing element approach, with the majority of them lower than 0.45 mm.
2. The three-dimensional ground disturbance was thoroughly analyzed. The numerical results displayed a symmetric distribution of the ground surface displacements. And the maximum surface displacement mainly occurred in the vertical direction. However, due to the dynamic excavation effect, there were some differences in the longitudinal direction. The longitudinal displacements of soil on the left side at the tunnel face were less than that on the right side. Additionally, as the jacking distance increased, the longitudinal displacement of the ground surface on the axis displayed a V-shape. This was in sharp contrast to the ground displacement. Specifically, as the pipe jacking machine advanced, the ground longitudinal displacement of the monitored section gradually increased. And the largest soil displacements were located on the axis. In addition, it was evident that the farther from

the jacking axis on the same cross-section, the smaller the longitudinal soil displacement.

3. The dynamic process of the excavated soil was clearly visualized. Specifically, after jacking began, the center cutter of the pipe jacking machine contacted the tunnel face, causing small deformations in the soil. As the cutter head fully contacted the tunnel face, the displacement of the soil increased. Finally, the cutter head completed a full rotation. The dynamic excavation process of the soil during this period was presented completely and explicitly. Moreover, the dynamic jacking process of the soil in the tunnel face at different times was also visualized. It was evident that during the jacking process, the gradual disappearance of the soil was well depicted. Additionally, the normal contact stress of the cutter head demonstrated that the numerical results aligned with the actual process of excavated soil being transferred into the soil screw conveyor.

Acknowledgement
The authors gratefully acknowledge financial supports for this research provided by the National Natural Science Foundation of China (Grant Number: 52208407, 52278416, U21A20152) and the fellowship of the China Postdoctoral Science Foundation (Grant Number: 2023T160543).

References
[1] Zhang, K., Zhang, X., Zhou, S., Zhang, Q., He, C. "Mechanical behavior and constitutive relationship of bond interface in steel plate-reinforced shield tunnels", Construction and Building Materials, 411, 134178, 2024. https://doi.org/10.1016/j.conbuildmat.2023.134178

[2] He, C., Cai, Y., Pu, C., Zhou, S., Di, H., Zhang, X. "Deformation analysis and protection measures of existing metro tunnels effected by river channel excavation in soft soils", Tunnelling and Underground Space Technology, 144, 105504, 2024. https://doi.org/10.1016/j.tust.2023.105504

[3] Jin, H., Yu, K., Gong, Q., Zhou, S. "Load-carrying capability of shield tunnel damaged by shield shell squeezing action during construction", Thin-Walled Structures, 132, pp. 69–78, 2018. https://doi.org/10.1016/j.tws.2018.07.057

[4] Alielahi, H., Feizi, D. "Numerical Study on Dynamic Effects of Soil-Tunnel-Structure Interaction", International Journal of Civil Engineering, 19(11), pp. 1339–1355, 2021. https://doi.org/10.1007/s40999-021-00642-8

[5] Ma, P., Shimada, H., Huang, S., Moses, D. N., Zhao, G., Ma, B. "Transition of the pipe jacking technology in Japan and investigation of its application status", Tunnelling and Underground Space Technology, 139, 105212, 2023. https://doi.org/10.1016/j.tust.2023.105212

[6] Hu, D., Zhou, R., Xiao, L., Liang, X., Li, Y., Yang, X. "A Super-shallow Buried Large-Span Rectangular Pipe Jacking Tunnel Undercrossing an Expressway: Construction Method, Monitoring Results, and Numerical Simulation", International Journal of Civil Engineering, 22(5), pp. 757–771, 2024. https://doi.org/10.1007/s40999-023-00908-3

[7] Milligan, G. W. E., Norris, P. "Site-based research in pipe jacking—objectives, procedures and a case history", Tunnelling and Underground Space Technology, 11, pp. 3–24, 1996. https://doi.org/10.1016/0886-7798(95)00041-0

[8] Peck, R. B. "Deep Excavations and Tunneling in Soft Ground: State-of-the-Art Report", In: 7th International Conference on Soil Mechanics and Foundation Engineering, Mexico City, Mexico, 1969, pp. 225–290.

[9] Niu, Z., Cheng, Y., Zhang, Y., Song, Z., Yang, G., Li, H. "A New Method for Predicting Ground Settlement Induced by Pipe Jacking Construction", Mathematical Problems in Engineering, 2020(1), 1681347, 2020. https://doi.org/10.1155/2020/1681347

[10] Beckmann, D., Stein, R., Fabri, T., Uhlenbroch, A. "CoJack – A new statics method of computing and controlling pipe jacking", Tunnelling and Underground Space Technology, 22(5–6), pp. 587–599, 2007. https://doi.org/10.1016/j.tust.2007.02.006

[11] Sun, W., Ding, X., Wei, J., Wang, X., Zhang, A. "Hierarchical modeling method and dynamic characteristics of cutter head driving system in tunneling boring machine", Tunnelling and Underground Space Technology, 52, pp. 99–110, 2016. https://doi.org/10.1016/j.tust.2015.11.022

[12] Ye, Y., Peng, L., Zhou, Y., Yang, W., Shi, C., Lin, Y. "Prediction of Friction Resistance for Slurry Pipe Jacking", Applied Sciences, 10(1), 207, 2020. https://doi.org/10.3390/app10010207

[13] Wei Liu, S., Zheng Zhao, S., Su, H., Zhu, Z. Q., Lai Qu, C. "Surface Deformation Law of Cixian Section of the South-to-North Water Transfer Project", IOP Conference Series: Earth and Environmental Science, 719(4), 042038, 2021. https://doi.org/10.1088/1755-1315/719/4/042038

[14] Choo, C. S., Ong, D. E. L. "Evaluation of Pipe-Jacking Forces Based on Direct Shear Testing of Reconstituted Tunneling Rock Spoils", Journal of Geotechnical and Geoenvironmental Engineering, 141(10), 04015044, 2015. https://doi.org/10.1061/(asce)gt.1943-5606.0001348

[15] Feng, X., Zhang, P., Chen, X., Zhang, Y., Ma, B., Liu, K., Xu, T., Zeng, C. "Field mechanical properties of large section concrete pipes during jacking in fractured moderately weathered siltstone", Tunnelling and Underground Space Technology, 131, 104818, 2023. https://doi.org/10.1016/j.tust.2022.104818

[16] Huang, X., Zhang, Q., Liu, Q., Liu, X., Liu, B., Wang, J., Yin, X. "A real-time prediction method for tunnel boring machine cutter-head torque using bidirectional long short-term memory networks optimized by multi-algorithm", Journal of Rock Mechanics and Geotechnical Engineering, 14(3), pp. 798–812, 2022. https://doi.org/10.1016/j.jrmge.2021.11.008

[17] Huo, J., Zhu, D., Hou, N., Sun, W., Dong, J. "Application of a small-timescale fatigue, crack-growth model to the plane stress/strain transition in predicting the lifetime of a tunnel-boring-machine cutter head", Engineering Failure Analysis, 71, pp. 11–30, 2017. https://doi.org/10.1016/j.engfailanal.2016.11.002

[18] Liu, X., Xiong, F., Zhou, X., Liu, D., Chen, Q., Zhang, J., Han, Y., Xu, B., Deng, Z., He, C. "Physical model test on the influence of the cutter head opening ratio on slurry shield tunnelling in a cobble layer", Tunnelling and Underground Space Technology, 120, 104264, 2022. https://doi.org/10.1016/j.tust.2021.104264

[19] Shen, S.-L., Zhang, N., Zhou, A. "Investigation of disc cutter wear during shield tunnelling in weathered granite: A case study", Tunnelling and Underground Space Technology, 140, 105323, 2023. https://doi.org/10.1016/j.tust.2023.105323

[20] Yang, S., Wang, M., Du, J., Guo, Y., Geng, Y., Li, T. "Research of jacking force of densely arranged pipe jacks process in pipe-roof pre-construction method", Tunnelling and Underground Space Technology, 97, 103277, 2020. https://doi.org/10.1016/j.tust.2019.103277

[21] Tang, L., Zhang, Z. "Using Retractable Baffle-Type Rectangular Pipe Jacking for the Construction of a Tunnel with a Large Cross-Section in a Complex Environment", International Journal of Civil Engineering, 22(6), pp. 901–923, 2024. https://doi.org/10.1007/s40999-023-00932-3

[22] Farrokh, E. "Cutter change time and cutter consumption for rock TBMs", Tunnelling and Underground Space Technology, 114, 104000, 2021. https://doi.org/10.1016/j.tust.2021.104000

[23] Li, M., Yang, J., Zeng, L., Jin, J., Liu, Y. "Case Study on the Interaction Between Rectangular Pipe Jacking Control and Ground Settlement in Silty Clay", International Journal of Civil Engineering, 21(9), pp. 1447–1462, 2023. https://doi.org/10.1007/s40999-023-00830-8

[24] Yu, B., Shimada, H., Sasaoka, T., Hamanaka, A., Matsumoto, F., Morita, T. "A jacking force study based on interpretation of box jacking records: A case study of curved rectangular box jacking in soft soil in Saitama, Japan", Tunnelling and Underground Space Technology, 139, 105228, 2023. https://doi.org/10.1016/j.tust.2023.105228

[25] Zhang, P., Zhang, Y., Ariaratnam, S. T., Ma, B., Zeng, C., Liu, K. "Field monitoring and analysis of soil deformation of curved steel pipe jacking in Gongbei tunnel", Tunnelling and Underground Space Technology, 138, 105153, 2023. https://doi.org/10.1016/j.tust.2023.105153

[26] Choo, C. S., Ong, D. E. L. "Assessment of non-linear rock strength parameters for the estimation of pipe-jacking forces. Part 2. Numerical modeling", Engineering Geology, 265, 105405, 2020. https://doi.org/10.1016/j.enggeo.2019.105405

[27] Han, X., Li, W., Chen, T., Liu, W. "Sensitivity analysis of ground settlement induced by pipe-jacking construction in soft soil stratum", E3S Web of Conferences, 136, 04028, 2019. https://doi.org/10.1051/e3sconf/201913604028

[28] Ramezanpour, M., Mir Mohammad Hosseini, S. M. "Numerical Simulation for the Estimation of the Critical Length of Steel Pipe Jacking in Alluvial Ground", Journal of Pipeline Systems Engineering and Practice, 13(4), 04022033, 2022. https://doi.org/10.1061/(asce)ps.1949-1204.0000669

[29] Ren, D.-J., Xu, Y.-S., Shen, J. S., Zhou, A., Arulrajah, A. "Prediction of Ground Deformation during Pipe-Jacking Considering Multiple Factors", Applied Sciences, 8(7), 1051, 2018. https://doi.org/10.3390/app8071051

[30] Gong, J., Zhang, K., Qi, P. "Numerical analysis on surface settlement in parallel rectangular pipe jacking construction", Journal of Physics: Conference Series, 2044(1), 012174, 2021. https://doi.org/10.1088/1742-6596/2044/1/012174

[31] Batsaikhan, U., Hashikawa, H., Shimada, H., Sasaoka, T., Hamanaka, A. "Numerical Study on the Applicability of the Pipe-Jacking Method for the Main Gate of an Underground Coal Mining in Weak Rock Mass", Applied Sciences, 12(3), 1719, 2022. https://doi.org/10.3390/app12031719

[32] Ma, W., Wang, B., Wang, X., Zhou, S., Wang, B. "Soil Layer Disturbance Caused by Pipe Jacking: Measurement and Simulation of a Case Study", KSCE Journal of Civil Engineering, 25(4), pp. 1467–1478, 2021. https://doi.org/10.1007/s12205-021-2262-4

[33] Zhang, C., Zhai, W., Xia, Y., Wang, C., Zhao, P., Li, B., Pan, Y., …, Chen, X. "Analysis of the stability of a novel assembled working shaft support structure during pipe jacking construction: Experiments and numerical simulations", Engineering Failure Analysis, 162, 108418, 2024. https://doi.org/10.1016/j.engfailanal.2024.108418

[34] Liu, K., Chen, X., Zhang, P., Ma, B., Feng, X., Zhang, Y., Liu, H., Tan, X., Xu, T. "Axial mechanical response of concrete pipe jacking considering the deflection of the bell-and-spigot joint: Full-scale test and numerical simulation", Tunnelling and Underground Space Technology, 149, 105805, 2024. https://doi.org/10.1016/j.tust.2024.105805

[35] Zhang, X., Shi, C., Sun, X. "Analysis of surface deformation characteristics in pipe jacking construction based on the theory of a stratum cross-correlation conditional random field", Computers and Geotechnics, 162, 105668, 2023. https://doi.org/10.1016/j.compgeo.2023.105668

[36] Li, X., Li, P., Liu, X., Sun, L., Cui, T., He, K., Guo, C. "Surface subsidence pattern of construction of pipe jacking in water-rich sand layer cross passage measured and numerical simulation analysis", Structures, 60, 105949, 2024. https://doi.org/10.1016/j.istruc.2024.105949

[37] Pan, Z., Du, K., Lv, F., Tao, S. "Numerical Simulation of Mechanical Response of Bridge Foundation and Existing Tunnel Caused by Pipe Jacking Construction", Journal of Physics: Conference Series, 2230(1), 012008, 2022. https://doi.org/10.1088/1742-6596/2230/1/012008

[38] Ko, D.-C., Kim, B.-M., Choi, J.-C. "Finite-element simulation of the shear process using the element-kill method", Journal of Materials Processing Technology, 72(1), pp. 129–140, 1997. https://doi.org/10.1016/S0924-0136(97)00144-1

[39] Padilla-Llano, D. A., Schafer, B. W., Hajjar, J. F. "Cyclic fracture simulation through element deletion in structural steel systems", Journal of Constructional Steel Research, 189, 107082, 2022. https://doi.org/10.1016/j.jcsr.2021.107082

[40] Wang, Y., Zhupanska O. I. "Modeling of thermal response and ablation in laminated glass fiber reinforced polymer matrix composites due to lightning strike", Applied Mathematical Modelling, 53, pp. 118–131, 2018. https://doi.org/10.1016/j.apm.2017.08.019

[41] Zhang, Y., Xin, H., Correia, J. A. F. O. "Fracture evaluation of ultra-high-performance fiber reinforced concrete (UHPFRC)", Engineering Failure Analysis, 120, 105076, 2021. https://doi.org/10.1016/j.engfailanal.2020.105076

[42] Han, M. D., Cai, Z. X., Qu, C. Y., Jin, L. S. "Dynamic numerical simulation of cutterhead loads in TBM tunnelling", Tunnelling and Underground Space Technology, 70, pp. 286–298, 2017. https://doi.org/10.1016/j.tust.2017.08.028

[43] Wang, J., Zhang, D., Chen, J., Fang, Q., Sun, Z., Lu, S. "A novel mechanics model for predicting vertical load and jacking force via rectangle pipe considering soil arching effect", Tunnelling and Underground Space Technology, 152, 105952, 2024. https://doi.org/10.1016/j.tust.2024.105952

[44] Zhang, R.-X., Su, D., Lin, X.-T., Zhu, T.-F., Lei, G., Chen, X.-S. "Investigation of the soil arching evolution in the ground with or without a tunnel", Transportation Geotechnics, 43, 101149, 2023. https://doi.org/10.1016/j.trgeo.2023.101149

[45] Chen, R.-P., Song, X., Meng, F.-Y., Wu, H.-N., Lin, X.-T. "Analytical approach to predict tunneling-induced subsurface settlement in sand considering soil arching effect", Computers and Geotechnics, 141, 104492, 2022. https://doi.org/10.1016/j.compgeo.2021.104492